

Oblique Incidence and Polarization Insensitive Multiband Metamaterial Absorber with Quad Paired Concentric Continuous Ring Resonators

Alkesh Agrawal^{1, *}, Mukul Misra¹, and Ashutosh Singh²

Abstract—Simulation and experimental measurement of a new design of an oblique incidence and polarization insensitive metamaterial absorber with multiband absorption is presented in this paper. The unit cell of the proposed metamaterial absorber comprises concentric continuous rings of different radii and widths placed in four different quadrants with identical pair of rings placed diagonally opposite, with each ring responsible for high absorption. The calculated dispersion behavior of MM absorber in terms of effective permittivity (ε_{eff}), effective permeability (μ_{eff}), and refractive index (η_{eff}) shows the metamaterial characteristics. The surface current and field distributions in MM absorber are simulated to understand the occurrence of absorption bands. The measured results show the absorption peaks of 99.5%, 99.8%, 99.5% and 99.9% at 7.20 GHz, 9.3 GHz, 12.61 GHz, and 13.07 GHz, respectively. The simulated results are well supported by the experimentally measured performance of the fabricated metamaterial absorber. It offers multiband absorption with bands lying in C-band, X-band and Ku-band for mobile communication, satellite communication and radar applications. With merged third and fourth absorption peaks, the proposed metamaterial absorber structure exhibits a broadband absorption.

1. INTRODUCTION

Metamaterials (MMs) are unnatural electromagnetic materials in which the electromagnetic properties are derived from the shape, size, periodicity and design of microscopic or nanoscopic structural units and not from the inherited material composition [1]. The material which exhibits the negative values of either permittivity ‘ ε ’ (ENG) or permeability ‘ μ ’ (MNG) or both (DNG) are characterized as left-handed materials (LHMs) by Veselago [2]. All the natural materials exhibit positive permittivity and positive permeability called double positive (DPS) and also termed as right-handed materials (RHMs). As the LHMs are usually not found naturally, they are termed as metamaterial. In order to practically realize metamaterial, Pendry et al. [3, 4] suggested to artificially engineer the metamaterials as the combination of periodic lattices of micro-structured wires as ENG material and split ring resonators (SRR) as MNG material.

In recent years, the study of metamaterials have been diversified to electromagnetic (EM) theory applied to Perfect Lens [5, 6], EM Cloak [7, 8], Microwave circuit application in MM Transmission Lines [9], Microwave Phase Shifters and Filters [10], Radiation applications in MM based Efficient Electrically Small Antennas [11], Composite Right-Left handed MM Antennas [12], MM based Patch Antennas [13], MM Perfect Absorbers [14–27], and MM THz waveguide [28].

The development of EM absorbers was initiated by Salisbury and Jaunmann [29] with the aim to improve radar performance and to provide concealment against enemy’s radar system. These

Received 13 June 2017, Accepted 9 August 2017, Scheduled 28 August 2017

* Corresponding author: Alkesh Agrawal (alkesh.ec@srmu.ac.in).

¹ Faculty of Electronics and Communication Engineering, Institute of Technology, Shri Ramswaroop Memorial University, Lucknow, India. ² Faculty of Physical Sciences, Institute of Natural Sciences and Humanities, Shri Ramswaroop Memorial University, Lucknow, India.

EM absorbers have a limitation of being thick and bulky. The improvement in EM absorbers led to researches in Metamaterial Perfect Absorber (MPA). Recent research work shows that MPAs find applications in reducing radar cross section (RCS) by absorbing radar echo thereby improving radar performance [30, 31], in improving antenna radiation pattern by absorbing undesired sidelobes [29], and in reducing electromagnetic interference (EMI) [30, 31] thereby reducing health hazards due to electromagnetic radiation exposure in mobile communication. Future applications include the use of MPA as selective thermal emitters [32] and wavelength sensitive sensors [33].

In this paper, a new design of MM absorber is proposed. The unit cell of the proposed MM absorber is composed of four pairs (quad paired) of concentric continuous rings (CCRs) with identical pairs of rings concentrated diagonally. The highly symmetric CCRs design is chosen to realize MM absorber insensitive to angle of incidence (θ), E -field and H -field variations (Φ), multiband and broadband absorption contributed by individual and combined effect of rings. The dimensions of the unit cell are optimized to achieve fairly good absorption by simulations using ‘CST microwave studio’. Finally, a periodic 10×10 matrix of the optimized unit cell is fabricated and tested in an anechoic chamber using vector network analyzer (VNA).

2. DESIGN AND SIMULATION OF THE MM ABSORBER

MPA is basically a three-layered structure consisting, on top, of an array of unit cells, constituting MM high impedance surface with metallic laminated ground plane separated by the dielectric [14]. An EM wave incident normally on top layer produces large E -field, H -field and surface currents, and gets absorbed to unity by the laminated resistive sheet at the bottom before reflecting back. MM lossy surface impedance must be matched with that of impedance of free space to achieve high absorbance by realizing the normalized impedance $Z(f)$ to ‘1’ by parametrically analyzing the MM structure. Recent research contributes to the development of multiband and broadband MPAs which are insensitive to E -field and H -field variations with wide angle of incidence of EM waves exhibiting multiband and broadband absorptions [14–27].

The proposed unit cell of the MM absorber consists of four sub-cells in four quadrants as shown in Fig. 1(a). Sub-cells 1 and 4 are identical and Sub-cells 2 and 3 are identical. Each sub-cell consists of a pair of concentric continuous rings. The pair of rings of Sub-cells 1 and 4 have the same width but different radii, and the pair of rings of Sub-cells 2 and 3 have different widths as well as different radii as shown in Figs. 1(b) and 1(c).

The optimum design parameters of the proposed MM absorber unit cell structure as given in Table 1 are realized on an FR-4 substrate (relative permittivity 4.4, loss tangent 0.02, and thickness 1.5 mm). The optimum design of MM absorber is simulated using CST Microwave studio suite, frequency domain solver of the code for normal incidence of the EM wave. Hexahedral meshing is used, and AR filter

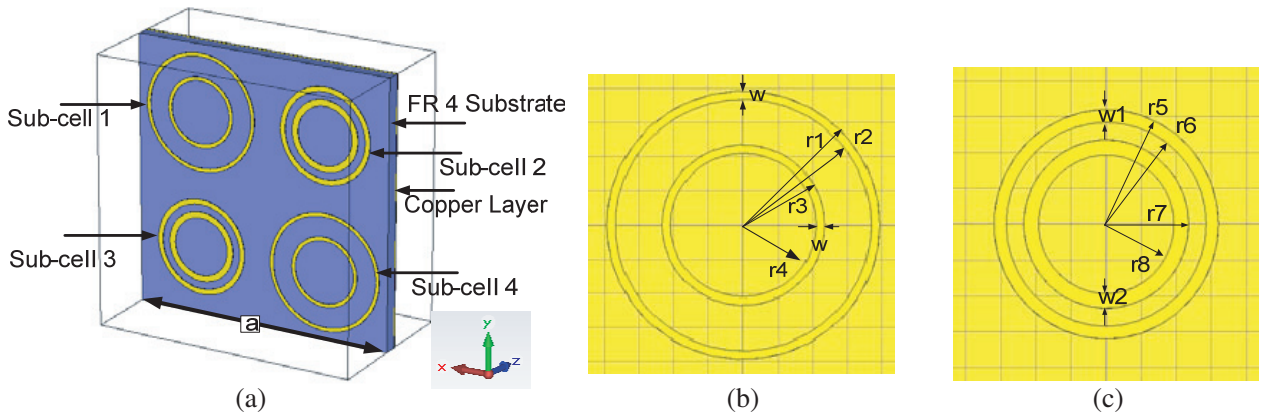


Figure 1. The geometry of a unit cell of MM absorber. (a) 3-D Perspective view. (b) Dimensions of rings of Sub-cells 1 and 4. (c) Dimensions of rings of Sub-cells 2 and 3.

module is adopted for the mesh refinement. The boundary conditions are shown in Fig. 2(a). Unit cell periodic boundary conditions are taken along x -direction and y -direction, and open boundary conditions are taken along the wave propagation direction, i.e., z -direction. The absorptivity is evaluated using Equation (1) [15–17],

$$A(f) = 1 - |S_{11}(f)|^2 - |S_{21}(f)|^2 \tag{1}$$

where $A(f)$ is the absorptivity, $|S_{11}(f)|^2$ the reflected power, and $|S_{21}(f)|^2$ the transmitted power of the incident electromagnetic radiation of frequency f . Since the proposed MM absorber structure consists of completely copper laminated bottom layer due to which the incident power is completely absorbed which reduces the value of $S_{21}(f)$ to zero, Equation (1) is modified to $A(f) = 1 - |S_{11}(f)|^2$. Therefore, absorptivity can be maximized by minimization of reflection from the top surface of the proposed MM structure. The geometrical parameters of the above mentioned unit cell structure as given in Table 1 are parametrically optimized to obtain high absorption at frequencies, which finds applications in C-band, X-band and Ku-band.

The simulated results for optimized MM absorber show that the absorptions peaks occur at 7.06 GHz, 9.18 GHz, 12.62 GHz and 13 GHz with absorptivities of 78%, 99.9%, 98.5% and 99.9%, respectively as shown in Fig. 2(b) for the normal incidence of EM waves.

To better understand the EM absorption behaviour of the MM absorber, surface current distributions, E -field orientation, and H -field orientation are simulated at all resonance frequencies

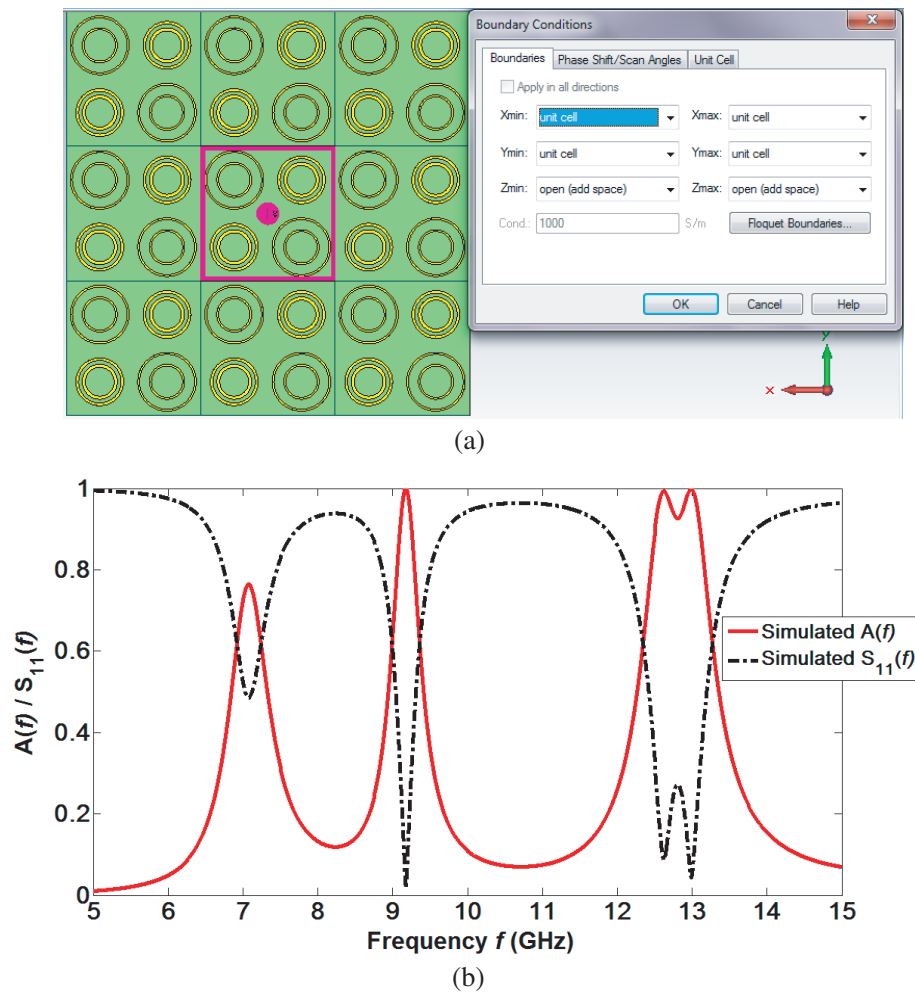
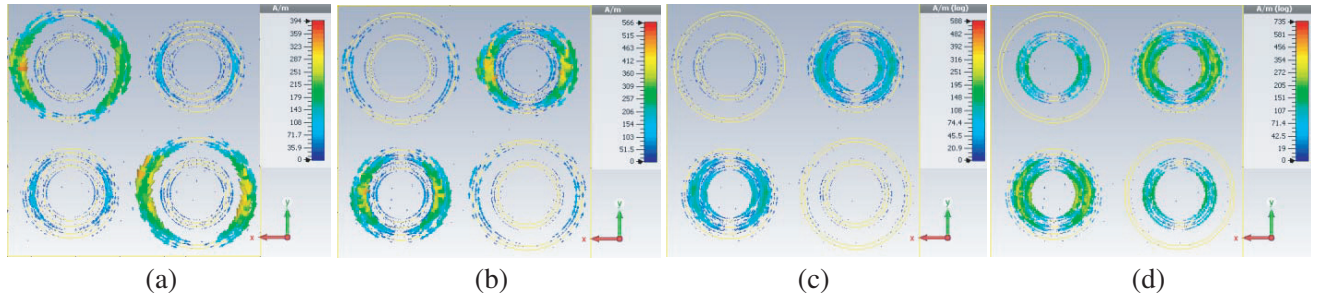
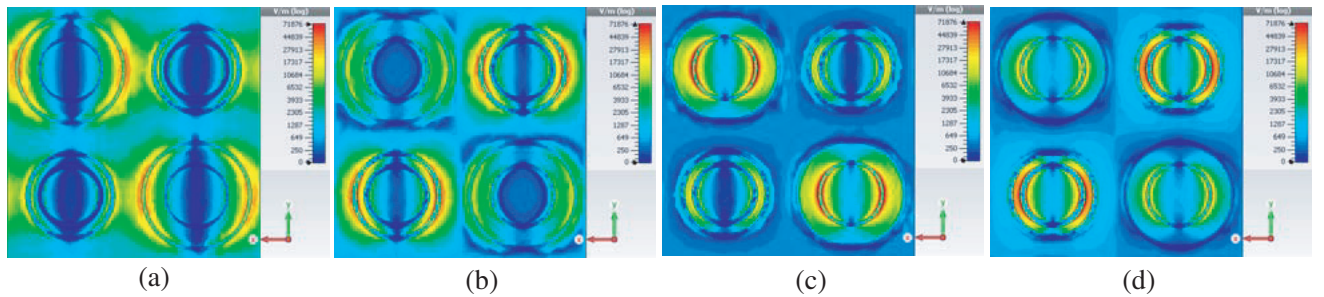


Figure 2. (a) Boundary conditions along the Unit cell of MM absorber structure. (b) Reflection coefficient $S_{11}(f)$ and Absorptivity $A(f)$ of the proposed MM structure.

Table 1. Optimized dimensions of unit cell.

Sub-cell 1 and Sub-cell 4		Sub-cell 2 and Sub-cell 3	
Element	Dimension (mm)	Element	Dimension (mm)
r_1	3.93	r_5	3.20
r_2	3.68	r_6	2.85
r_3	2.35	r_7	2.35
r_4	2.10	r_8	1.93
w	0.25	w_1	0.35
		w_2	0.42

as shown in Figs. 3, 4, and 5, respectively. When time varying EM waves are incident normally on the MM absorber parallel to the axis of the concentric continuous circular rings, surface currents are induced, which depends on the resonant properties of the MM absorber at different resonant frequencies as shown in Fig. 3. The arrow indicates the direction of flow of induced surface current, and the color indicates the intensity. The induced currents produce magnetic field that further supports or opposes the incident field. Each continuous ring behaves as a resonator that resonates at a particular frequency where absorption takes place shown in Fig. 3. The periodic array of the unit cell which comprises quad paired concentric circular rings results in strong coupling between the resonator structures that further results in high absorption of incident EM waves as shown in Fig. 3. As a result, unique properties in terms of negative permeability and negative permittivity arise from the composite MM absorber structure. The E -field and H -field become more prominent at the absorption peaks shown in Figs. 4 and 5. Since E -field and H -field are perpendicular to each other, E -field gets concentrated along $+x$ and $-x$ directions along different rings of the sub-cells as shown in Fig. 4, and H -field is concentrated along

**Figure 3.** Surface current distributions at the top layer of the proposed MM absorber at frequencies of absorption. (a) 7.06 GHz. (b) 9.18 GHz. (c) 12.62 GHz. (d) 13 GHz.**Figure 4.** Electric field distributions in proposed MM absorber at frequencies of absorption. (a) 7.06 GHz. (b) 9.18 GHz. (c) 12.62 GHz. (d) 13 GHz.

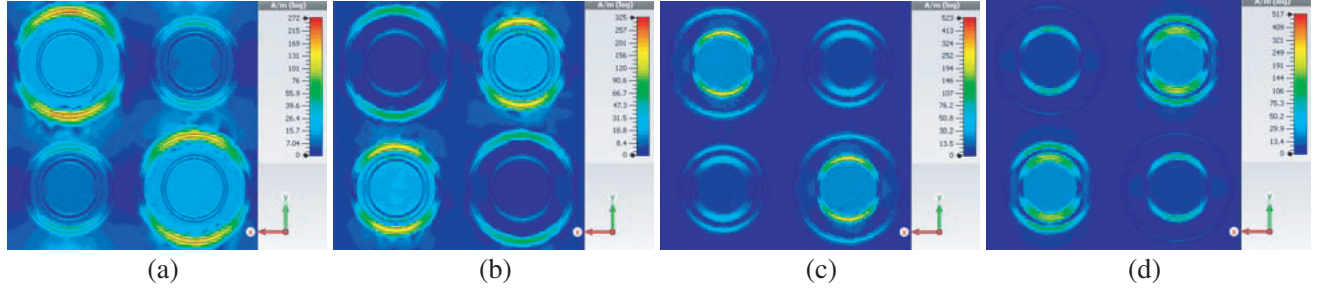


Figure 5. Magnetic field distributions in proposed MM absorber at frequencies of absorption. (a) 7.06 GHz. (b) 9.18 GHz. (c) 12.62 GHz. (d) 13 GHz.

$+y$ and $-y$ directions along different rings as shown in Fig. 5. The energy of the H -field is concentrated on the metallic ring which acts as an inductive element and responsible for magnetic resonance, and similarly, the E -field is concentrated in between the metallic rings where the gaps act as capacitive elements and responsible for electric resonance. The individual rings responsible for the absorption at the distinct frequencies are identified from the surface current distributions, the E -field and H -field orientations. For the first resonance frequency, the surface current distribution, E -field and H -field orientations are along outer rings of the first and fourth sub-cells. For the second resonance frequency, the surface current distribution, E -field and H -field orientations are along outer rings of the second and third sub-cells. For the third resonance frequency, the surface current distribution, E -field and H -field orientations are along inner rings of the second and third sub-cells. For the fourth resonance frequency, the surface current distribution, E -field and H -field orientations are along inner rings of all the sub-cells.

The MM absorber structure is studied for the effect of variations of angle of incidence (θ) and variations of E -field and H -field orientations (Φ) on absorptivity at different absorption bands through simulations as well as experiment.

3. METAMATERIAL PROPERTIES OF MM ABSORBER

The metamaterial behavior of the proposed MM absorber is studied by calculating the dispersion characteristics of the simulated S -parameters for which many standard methods are used such as Nicolson Rose Weir (NRW) method [34], Transmission-Reflection (TR) method [35] and a more recent Direct Refractive Index (DRI) method [36]. These methods require reflection (S_{11}) and transmission (S_{21}) parameters for direct calculations of effective impedance (Z_{eff}), effective permittivity (ϵ_{eff}), effective permeability (μ_{eff}) and refractive index (η_{eff}).

Equation (2) [20] is used to calculate the variations of normalized impedance Z , with incident EM wave for the proposed MM absorber shown in Fig. 6. It is observed that the real part of normalized impedance is near unity [$\text{Re}(Z) \approx 1$], and imaginary part is close to zero [$\text{Im}(Z) \approx 0$] which indicates impedance matching of proposed MM absorber with that of free space.

$$Z = \sqrt{\frac{(1 + S_{11})^2 - S_{21}^2}{(1 - S_{11})^2 - S_{21}^2}} \quad (2)$$

According to NRW method, μ_{eff} and ϵ_{eff} are given by Equations (5) and (6), respectively, where d is the thickness of the substrate and k_o the wave number [36].

$$V_1 = S_{21} + S_{11} \quad (3)$$

$$V_2 = S_{21} - S_{11} \quad (4)$$

$$\mu_{eff} = \frac{2}{jk_0d} \left(\frac{1 - V_2}{1 + V_2} \right) \quad (5)$$

$$\epsilon_{eff} = \frac{2}{jk_0d} \left(\frac{1 - V_1}{1 + V_1} \right) \quad (6)$$

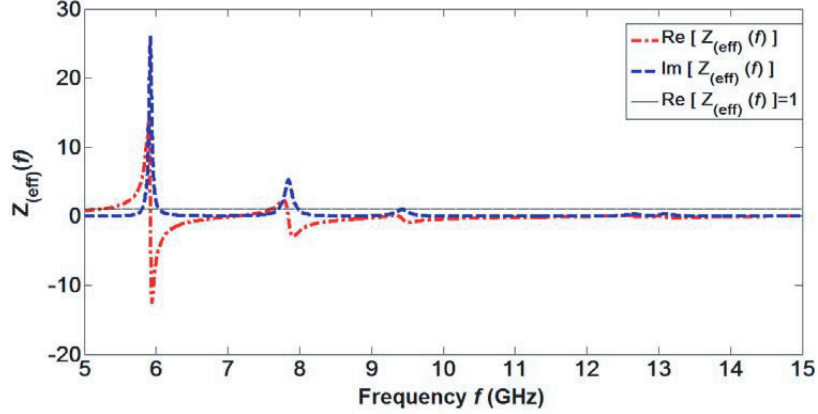


Figure 6. Variations of $\text{Re}[Z_{\text{eff}}]$ and $\text{Im}[Z_{\text{eff}}]$ with frequency.

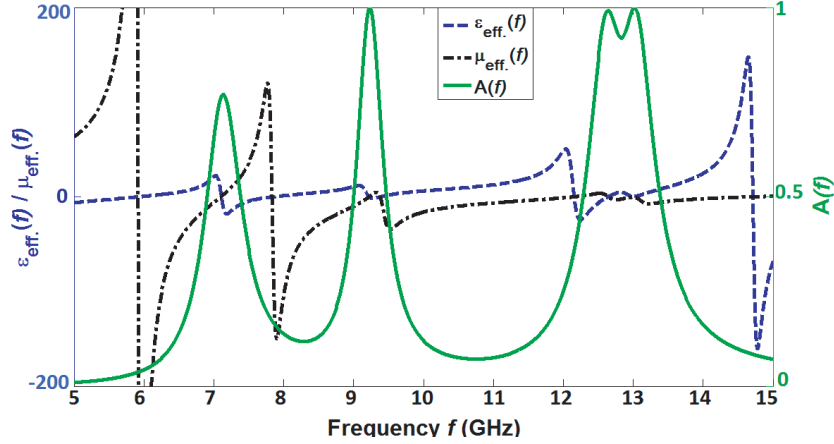


Figure 7. Variations of effective permittivity and permeability with frequency using Nicolson Ross Weir method (NRW).

$$\eta = \sqrt{\mu_{\text{eff}} \varepsilon_{\text{eff}}} \quad (7)$$

The calculated values of μ_{eff} and ε_{eff} by NRW method are shown in Fig. 7. It can be seen in Fig. 7 that the dispersion behaviors of both μ_{eff} and ε_{eff} show transitions and have negative values in the vicinity or within the absorption peaks for the MM absorber, thus showing metamaterial behavior. In order to reconfirm the dispersion of ε_{eff} and μ_{eff} , η_{eff} of the proposed MM absorber is calculated by NRW method using Equation (7) and compared with the directly calculated η using Equation (8) of DRI method proposed by Islam et al. [36].

$$\eta \approx \frac{c}{j\pi f d} \left(\frac{(S_{21} - 1)^2 - S_{11}^2}{(S_{21} + 1)^2 - S_{11}^2} \right)^{\frac{1}{2}} \quad (8)$$

where f is the frequency and d the thickness of the substrate.

A comparison of the η calculated by NRW method and DRI method for the proposed MM absorber is shown in Fig. 8. The dispersion characteristics of η calculated by the two methods are in good agreement which further confirms the metamaterial behavior of the proposed MM absorber.

4. EXPERIMENT

A 10×10 periodic matrix of optimized unit cell ($18 \text{ mm} \times 18 \text{ mm}$) is fabricated on an FR-4 substrate (relative permittivity 4.4, loss tangent 0.02, and thickness 1.5 mm) by conventional UV photolithography

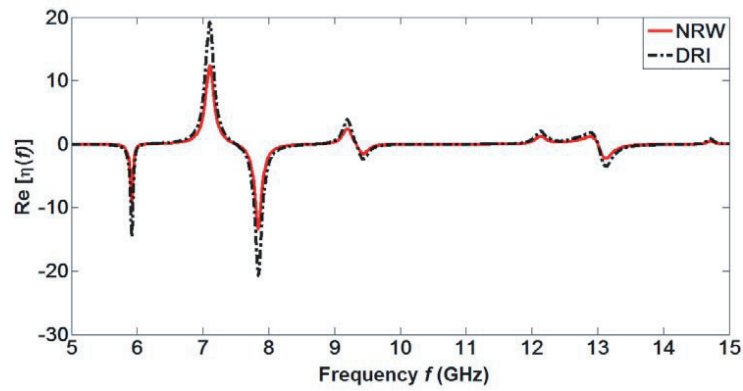


Figure 8. Variations of effective refractive index with frequency using Nicolson Ross Weir (NRW) method and Direct Refractive Index (DRI) method.

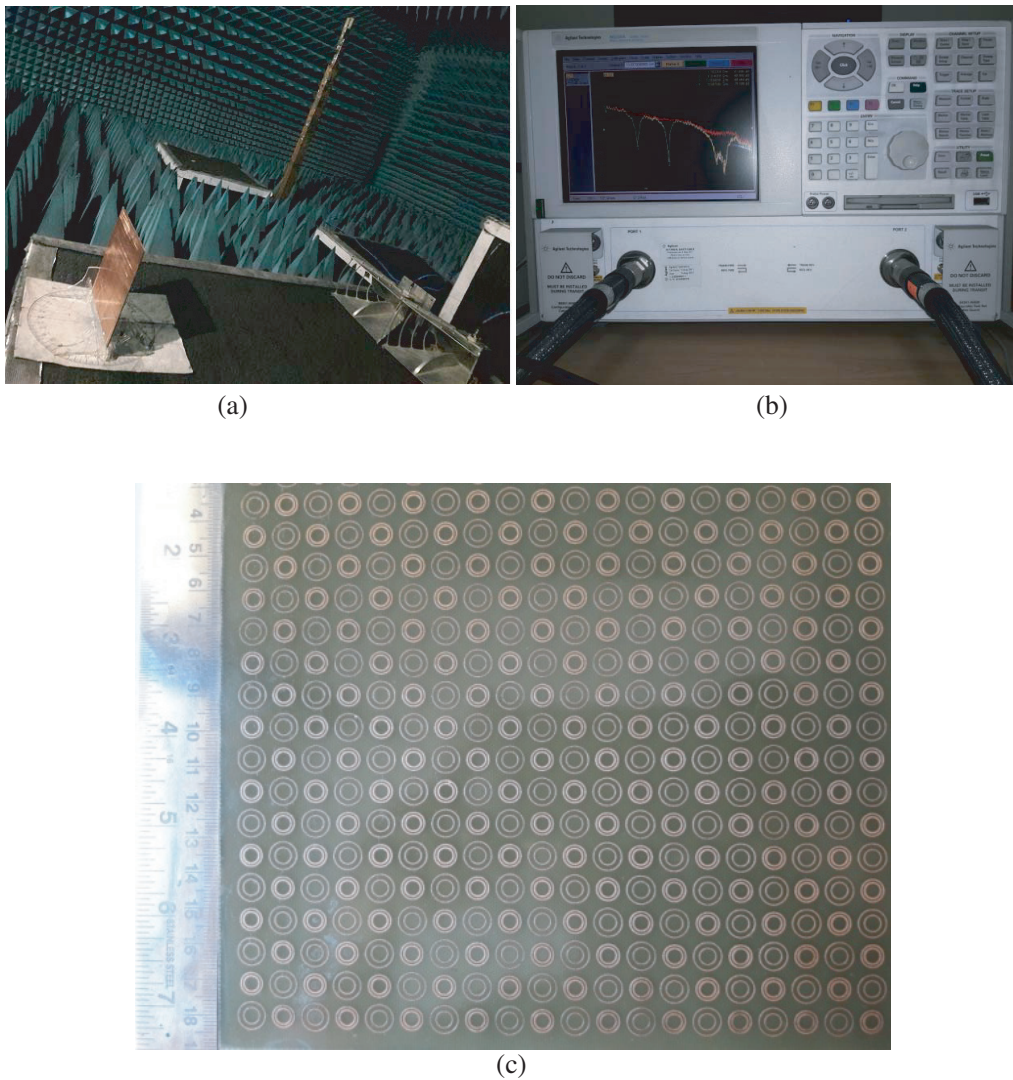


Figure 9. (a) Experimental setup. (b) Vector Network Analyzer (Agilent Technologies N5230A, 10 MHz–50 GHz). (c) The fabricated MM absorber structure of dimension 180 mm × 180 mm consisting 100 Unit cells.

followed by wet etching. The fabrication process started with the creation of mask from the Gerber file on the translucent paper. A positive photo resist is spin-coated (1200 rpm for two minutes) on one side of the substrate and baked at 100°C for 25 minutes. The photo-resist side is then exposed to UV radiation through the mask for 15 minutes. The desired pattern is developed using developing agent, and after this the substrate is post baked for 25 minutes at 100°C . The other Cu side of the substrate is protected by photo resist. Finally, the Cu etching of the developed pattern is done in FeCl_3 solution. After etching, the desired pattern of concentric continuous Cu rings appears on one side of the FR-4 substrate in $180\text{ mm} \times 180\text{ mm}$ area as shown in Fig. 9(c).

The fabricated MM absorber is placed inside an anechoic chamber in front of side by side placed transmitting and receiving horn antennas capable of transmitting and receiving EM waves up to 20 GHz as shown in Fig. 9(a). Both transmitting and receiving horn antennas are connected by low loss co-axial cables to a Vector Network Analyzer (Agilent Technologies N5230A, 10 MHz–50 GHz) placed outside the anechoic chamber as shown in Fig. 9(b).

The position of the MM absorber under consideration in front of the transmitting and receiving horn antennas is decided to minimize the influence of near-field and diffraction effects on the measurements. The distance of MM absorber $D = 1\text{ m}$ from antennas is chosen as measured dimension of the fabricated MM absorber structure and is approximated to 4.5λ (λ is the operating wavelength corresponding to the lowest frequency) which is much larger than $2D^2/\lambda$ [37].

In order to calibrate the measurement process, the simple copper ground plane of MM absorber is placed at a fixed 1 m distance facing the transmitting and receiving horn antennas, and S_{11} is measured and saved. Thus the reflection parameter S_{11} for a simple copper sheet of the size of MM absorber is measured for the experimental configuration. Next, the copper ground plane of MM absorber structure is rotated by 180° at the same position so that the fabricated concentric continuous rings structure now faces the transmitting and receiving horn antennas, and again the S_{11} is measured and saved by the VNA. The difference of the two measurements (from the copper laminated side and the MM absorber structure side) gives the actual S_{11} from the MM absorber structure as shown in Fig. 10.

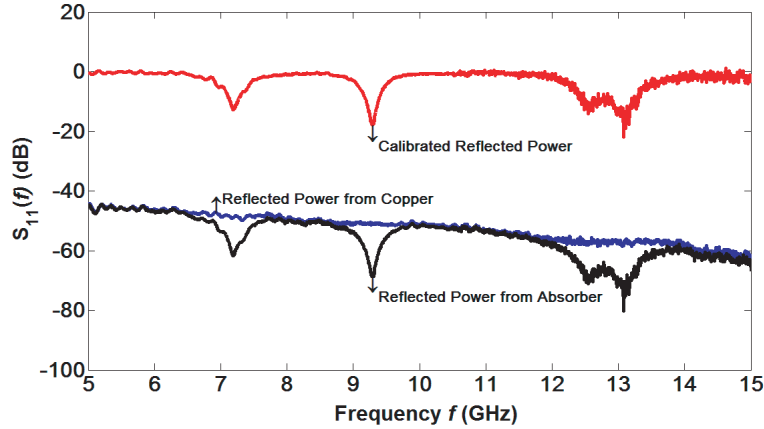


Figure 10. Measured reflected power as a difference of power reflected from Cu laminated FR-4 surface and MM absorber surface.

It can be seen that the measured S_{11} absorption peaks in Fig. 10 are at frequencies 7.20 GHz, 9.3 GHz, 12.61 GHz, and 13.07 GHz, which are the same as those predicted by simulation shown in Fig. 2(b).

5. RESULTS

The experimentally measured values of S_{11} and estimated absorptivity for normal incidence, oblique incidence EM radiation as well as for normally incident EM radiation with varying angle of polarization on MM absorber are compared with the simulated results. Fig. 11(a) and Fig. 11(b) respectively show

the S_{11} and absorptivity of the MM absorber for normally incident EM radiation. The experimentally measured frequencies of absorption bands are slightly on the higher side, and the measured bandwidths of the absorption bands is larger than simulated values. It may be attributed to the slight variations in the geometries of fabricated concentric continuous copper rings on large MM absorber structure (180 mm \times 180 mm) by conventional UV photolithography followed by wet etching process. The experimental results show that the absorptivity is more than 99.5% for all absorption peaks in all the absorption bands at frequencies, first at 7.20 GHz (99.5%), second at 9.3 GHz (99.9%), third at 12.61 GHz (99.5%) and fourth at 13.07 GHz (99.9%) as shown in Fig. 11(b). The third and fourth absorption peaks are merged to generate a broadband ($f_H = 13.4$ GHz and $f_L = 12.2$ GHz) of 3 dB bandwidth of 1.2 GHz in the Ku-band.

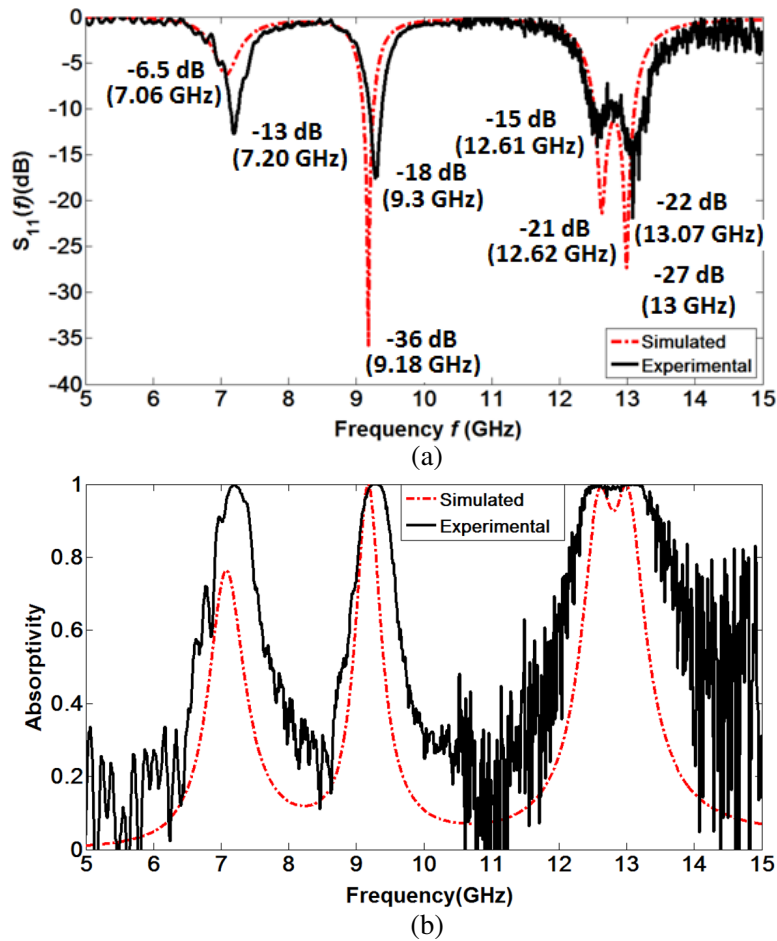


Figure 11. (a) Comparison of simulated and measured values of S_{11} and resonance peaks. (b) Simulated and measured values of absorptivities in the proposed MM absorber structure.

Figure 12(a) shows the schematic for the measurement of absorptivity as a function of angle of polarization (Φ) for normally incident EM radiation. Figs. 12(b) and 12(c) respectively show the simulated and experimentally measured absorptivities of the MM absorber for various angles of polarization (Φ). In the simulated results shown in Fig. 12(b), the absorptivity of the absorption bands does not change with angle of polarization (Φ). The measured absorptivities of the MM absorber for the angles of polarization $\Phi = 0^\circ$, $\Phi = 15^\circ$, and $\Phi = 30^\circ$ also show the polarization insensitivity under normal incidence due to the symmetrical design of MM absorber structure.

Similarly, Fig. 13(a) shows the schematic for the measurement of absorptivity as a function of angle of incidence (θ) for obliquely incident EM waves. The simulated and experimentally measured

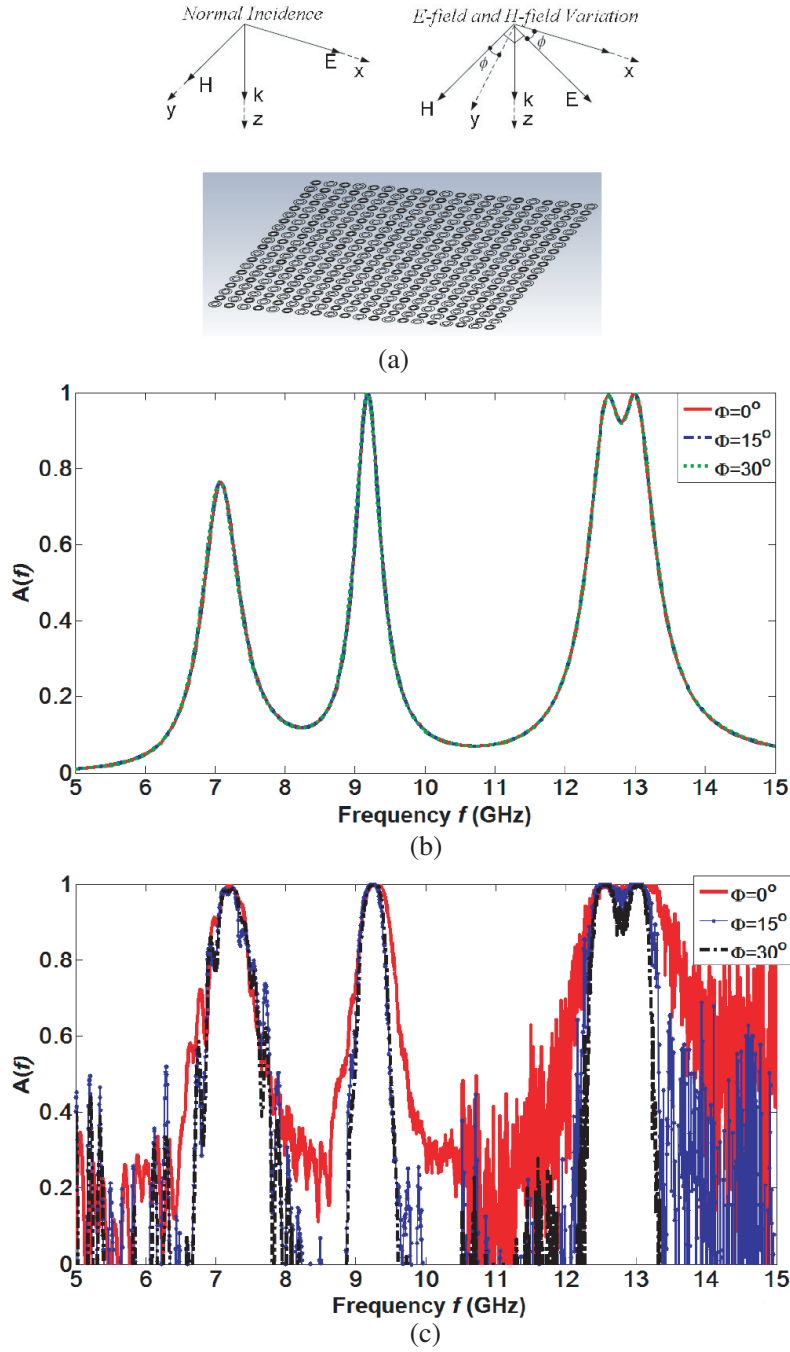


Figure 12. (a) Arrangement of the MM absorber structure for S_{11} measurements under E -field and H -field variations. (b) Simulated and (c) measured absorptivities for various E -field and H -field orientations of EM waves (Φ).

absorption peaks at different resonance frequencies for $\theta = 0^\circ$, $\theta = 15^\circ$, $\theta = 30^\circ$, and $\theta = 45^\circ$ are shown in Figs. 13(b) and 13(c), respectively. The measured absorptivities for various angles of incidence are in good agreement with the simulated absorptivities for the same angles of incidence. The proposed MM absorber shows high absorbance with change in angle of incidence for $\theta = 0^\circ$, $\theta = 15^\circ$, $\theta = 30^\circ$, and $\theta = 45^\circ$ is also contributed by the symmetrical design of the proposed MM absorber.

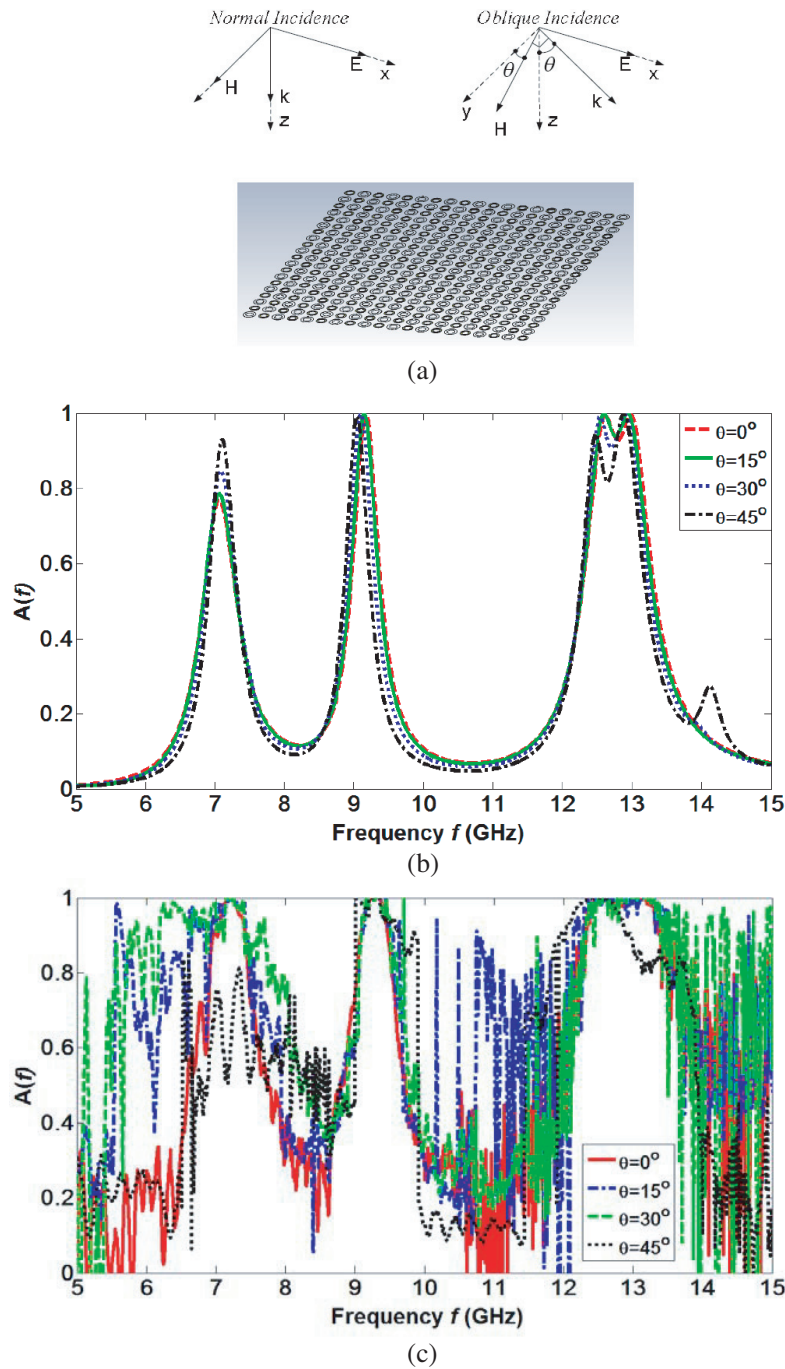


Figure 13. (a) Arrangement of the MM absorber structure for S_{11} measurements under normal and oblique angle of incidence. (b) Simulated and (c) measured absorptivities for different angles of incidence of EM waves (θ).

6. DISCUSSION

The simulated and experimentally measured results tabulated in Table 2 show that the measured resonance frequencies have a minor deviations in values of occurrence with that of simulated resonance frequencies. The measured value of S_{11} (-13 dB) at the first resonance frequency is numerically greater than the simulated value of S_{11} (-6.5 dB). At all other resonance frequencies, the simulated value of S_{11}

is found to be numerically greater than the measured value. The experimentally measured absorptivity at the first resonance frequency 7.20 GHz is found considerably higher (99.5%) than the simulated value of absorption (78%), due to over etching of outer rings of Sub-cells 1 and 4. The simulation results also support the fact that the reduction in the width ($r_1 - r_2$) of the outer rings of Sub-cells 1 and 4 appreciably increases the absorptivity at the first resonance frequency 7.20 GHz. At all other resonance frequencies, the measured absorptivities are same as the simulated values. The minor deviations in the numerical values of frequencies of resonance, reflected power and absorptivities in measured and simulated results are because the proposed MM absorber is wet etched. The measured and simulated results could be closer if the proposed MM absorber was dry etched.

Table 2. Simulated vs measured results.

Simulated Results			Experimental Results		
Resonance Frequency (GHz)	S_{11} (dB)	Absorptivity	Resonance Frequency (GHz)	S_{11} (dB)	Absorptivity
7.06	-6.5	78%	7.20	-13	99.5%
9.18	-36	99.9%	9.3	-18	99.9%
12.62	-21.5	98.5%	12.61	-15	99.5%
13	-27.5	99.9%	13.07	-22	99.9%
Broadband Bandwidth: 1.1 GHz			Broadband Bandwidth: 1.2 GHz		

The measured values of S_{11} and estimated absorptivities at oblique incidence (θ) and varied polarization angle (Φ) show the undesired noisy components. It may be because the dimensions of the proposed MM absorber structure (180 mm \times 180 mm) are comparably smaller than the aperture of the transmitting horn antenna, and as a result, a significant amount of generated power from the transmitting horn antenna might be diffracted and scattered from the cornered sections of the MM absorber structure.

7. CONCLUSION

A new design of MM absorber has been proposed in which each unit cell consists of four pairs of continuous concentric rings in four quadrants, with identical pair of rings fixed diagonally. The radii and widths of the continuous concentric rings in the proposed MM absorber are optimized in such a way that it provides maximum absorption of the received signal at different resonance frequencies. The proposed MM absorber is simulated in CST microwave studio, fabricated and experimentally tested to validate the results obtained from simulation. Results obtained from simulation are in close agreement with those obtained experimentally. The measured results show that the absorptions of 99.5%, 99.9%, 99.5% and 99.9% are achieved at 7.20 GHz, 9.3 GHz, 12.61 GHz, and 13.07 GHz respectively. The third and fourth absorption peaks are merged to give a broadband absorption of 1.2 GHz (12.2 GHz–13.4 GHz). ϵ_{eff} , μ_{eff} and η_{eff} are calculated to study and verify the metamaterial behavior of proposed MM absorber. EM response in terms of surface current distributions, E -field and H -field orientations along x and y directions are observed to study and identify the resonating behavior of the individual ring at distinct frequency of operation. Each ring in the structure of a unit cell is found responsible for absorption at a distinct resonance frequency, where the third and fourth resonance frequencies are merged to produce a broadband absorption contributed by inner rings of all four quadrants. The proposed MM absorber is investigated for the effect of variation in angle of incidence (θ) and E -field and H -field orientations (Φ) on absorptivity. The simulated and measured results show that the MM absorber is insensitive to angle of incidence and polarization insensitive for multiband as well as broadband absorptions suitable for mobile communication, satellite communication and radar applications in C-band, X-band and Ku-band.

ACKNOWLEDGMENT

The authors are highly thankful to Prof. (Dr.) P. K. Jain, Center of Research in Microwave Tubes, Department of Electronics Engineering, IIT (BHU) Varanasi and Prof. (Dr.) K. V. Srivastava, Department of Electrical Engineering, IIT Kanpur for providing the required facilities to carry out the present research work.

REFERENCES

1. Kshetrimayum, R. S., "A brief intro to metamaterials," *IEEE Potentials*, Vol. 23, No. 5, 44–46, 2004.
2. Veselago, V. G., "The electrodynamics of substances with simultaneously negative values of ϵ and μ ," *Soviet Physics Uspekhi*, Vol. 10, No. 4, 509–514, 1968.
3. Pendry, J. B., A. J. Holden, W. J. Stewart, and I. Youngs, "Extremely low frequency plasmons in metallic mesostructures," *Phys. Rev. Lett.*, Vol. 76, No. 25, 4773–4776, 1996.
4. Pendry, J. B., A. J. Holden, D. J. Robbins, and W. J. Stewart, "Magnetism from conductors and enhanced nonlinear phenomena," *IEEE Trans. Microwave Theory Tech.*, Vol. 47, No. 11, 2075–2084, 1999.
5. Pendry, J. B., "Negative refraction makes a perfect lens," *Phys. Rev. Lett.*, Vol. 85, No. 18, 3966–3969, 2000.
6. Fang, N., H. Lee, C. Sun, and X. Zhang, "Sub-diffraction-limited optical imaging with a silver superlens," *Science*, Vol. 308, 534–537, 2005.
7. Pendry, J. B., D. Schurig, and D. R. Smith, "Controlling electromagnetic fields," *Science*, Vol. 312, 1780–1782, 2006.
8. Schurig, D., J. J. Mock, B. J. Justice, S. A. Cummer, J. B. Pendry, A. F. Starr, and D. R. Smith, "Metamaterial electromagnetic cloak at microwave frequencies," *Science*, Vol. 314, 977–980, 2006.
9. Sanada, A., C. Caloz, and T. Itoh, "Characterization of the composite right/left handed transmission lines," *IEEE Microwave Wireless Components Letters*, Vol. 14, 280–282, 2004.
10. Nefedov, I. S. and S. A. Tretyakov, "On potential applications of metamaterials for the design of broadband phase shifters," *Microwave Optical Technology Letters*, Vol. 45, 98–103, 2005.
11. Ziolkowski, R. W., "Metamaterial-based efficient magnetically small antennas," *IEEE Transactions on Antennas and Propagation*, Vol. 54, No. 7, 2006.
12. Caloz, C., S. Abielmona, H. V. Nguyen, and A. Rennings, "Dual composite right-/left-handed (D-CRLH) leaky-wave antenna with low beam squinting and tunable group velocity," *Phys. Stat. Solidi (b)*, Vol. 244, 1219–1226, 2007.
13. Alu, A., F. Billoti, N. Engheta, and L. Vegni, "Sub-wavelength, compact, resonant patch antennas loaded with metamaterials," *IEEE Transactions Antenna Propagation*, Vol. 3, 882–891, 2007.
14. Landy, N. I., S. Sajuyigbe, J. J. Mock, D. R. Smith, and W. J. Padilla, "Perfect metamaterial absorber," *Physical Review Letters*, Vol. 100, 207402, 2008.
15. Bhattacharyya, S. and K. V. Srivastava, "An ultra thin magnetic field driven LC resonator structure as metamaterial absorber for dual band applications," *Proceedings International Symposium on Electromagnetic Theory*, 722–725, 2013.
16. Bhattacharyya, S., H. Baradiya, and K. V. Srivastava, "An ultra thin metamaterial absorber using magnetic field driven LC resonator with meander lines," *IEEE International Symposium on Antennas and Propagation and USNC/URSI National Radio Science Meeting, Chicago, USA*, 1–2, Jul. 8–13, 2012 .
17. Bhattacharyya, S., S. Ghosh, and K. V. Srivastava, "Triple band polarization-independent metamaterial absorber with bandwidth enhancement at X-band," *Journal of Applied Physics*, Vol. 114, 094514, 2013.
18. Wang, B. X., L. L. Wang, G. Z. Wang, W. Q. Huang, X. F. Li, and X. Zhai, "Theoretical investigation of broadband and wide-angle terahertz metamaterial absorber," *IEEE Photonics Technology Letters*, Vol. 26, No. 2, 111–114, Jan. 15, 2014.

19. Ayop, O., M. K. A. Rahim, and N. A. Samsuri, "Dual band polarization insensitive and wide angle circular ring metamaterial absorber," *8th European Conference on Antennas and Propagation (EuCAP)*, 955–957, 2014.
20. Agarwal, M., A. K. Behera, and M. K. Meshram, "Wide-angle quad-band polarization insensitive metamaterial absorber," *Electronics Letters*, Vol. 52, No. 5, 340–342, 2016.
21. Che Seman, F. and R. Cahill, "Frequency selective surfaces based planar microwave absorbers," *PIERS Proceedings*, 906–909, Kuala Lumpur, Malaysia, Mar. 27–30, 2012.
22. Huang, L. and H. Chen, "Multi-band and polarization insensitive metamaterial absorber," *Progress In Electromagnetics Research*, Vol. 113, 103–110, 2011.
23. Li, M. H., H. L. Yang, and X. W. Hou, "Perfect metamaterial absorber with dual bands," *Progress In Electromagnetics Research*, Vol. 108, 37–49, 2010.
24. Chettiar, U. K., A. V. Kildishev, H. Yuan, W. Cai, S. Xiao, V. P. Drachev, and V. M. Shalaev, "Dual-band negative index metamaterial: Double negative at 813nm and single negative at 772 nm," *Optical Letters*, Vol. 32, 1617, 2007.
25. Dincer, F., M. Karaaslan, E. Unal, and C. Sabah, "Dual-band polarization independent metamaterial absorber based on omega resonator and octa-starstrip configuration," *Progress In Electromagnetics Research*, Vol. 141, 219–231, 2013.
26. Dincer, F., M. Karaaslan, E. Unal, O. Akgol, E. Demirel, and C. Sabah, "Polarization and angle independent perfect metamaterial absorber based on discontinuous cross-wire-strips," *Journal of Electromagnetic Waves and Applications*, Vol. 28, No. 6, 741–751, 2014.
27. Dincer, F., M. Karaaslan, S. Colak, E. Tetik, O. Akgol, O. Altıntas, and C. Sabah, "Multi-band polarization independent cylindrical metamaterial absorber and sensor application," *Modern Physics Letters B*, Vol. 30, No. 8, 1650095, 2016.
28. Williams, C. R., M. Misra, S. R. Andrews, S. A. Maier, S. Carretero-Palacios, S. G. Rodrigo, F. J. Garcia-Vidal, and L. Martin-Moreno, "Dual band terahertz waveguiding on a planar metal surface patterned with annular holes," *Appl. Phys. Lett.*, Vol. 96, 011101, 2010.
29. Salisbury, W. W., "Absorbent body for electromagnetic waves," *United States Patent 2599944*, 1954
30. Motevasselian, A. and B. L. G. Jonsson, "Radar cross section reduction of aircraft wing front end," *Proceedings IEEE International Conference on Electromagnetics in Advanced Applications (ICEAA '09)*, 237–240, Turin, Italy, 2009.
31. Emerson, W. H., "Electromagnetic wave absorbers and anechoic chambers through the years," *IEEE Transactions on Antennas and Propagation*, Vol. 21, No. 4, 484–490, 1973.
32. Liu, X., T. Tyler, T. Starr, A. F. Starr, N. M. Jokerst, and W. J. Padilla, "Taming the blackbody with infrared metamaterials as selective thermal emitters," *Physical Review Letters*, Vol. 107, 045901, 2011.
33. Maier, T. and H. Brueckl, "Wavelength-tunable microbolometers with metamaterial absorbers," *Optical Letters*, Vol. 34, 3012–3014, 2009.
34. Luukkonen, O., S. I. Maslovski, and S. A. Tretyakov, "A stepwise Nicolson-Ross-Weir based material parameter extraction method," *IEEE Antenn. Wirel. Prop. Lett.*, Vol. 10, 1295–1298, 2011.
35. Baker-Jarvis, J., E. J. Vanzura, and W. A. Kissick, "Improved technique for determining complex permittivity with the transmission/reflection method," *IEEE Trans. Microw. Theory Tech.*, Vol. 38, 1096–1103, 1990.
36. Islam, S. S., M. R. I. Faruque, and M. T. Islam, "A new direct retrieval method of refractive index for the metamaterial," *Current Science*, Vol. 109, 337–342, 2015.
37. Balanis, C. A., *Antenna Theory: Analysis and Design*, 3rd Edition, Ch. 2, 34, 2005.